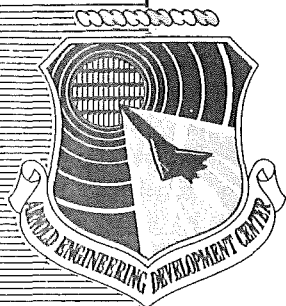# Laser-Raman Flow-Field Diagnostics of Two Large Hypersonic Test Facilities

W. D. Williams, D. A. Wagner,
H. M. Powell, and L. L. Price
ARO, Inc.

December 1979

Final Report for Period April 13, 1977 — July 10, 1978

TECHNICAL REPORTS
FILE COPY

Approved for public release; distribution unlimited.

ARNOLD ENGINEERING DEVELOPMENT CENTER
ARNOLD AIR FORCE STATION, TENNESSEE
AIR FORCE SYSTEMS COMMAND
UNITED STATES AIR FORCE

This report has been reviewed by the Information Office (OI) and is releasable to the National Technical Information Service (NTIS). At NTIS, it will be available to the general public, including foreign nations.

APPROVAL STATEMENT

This report has been reviewed and approved.

KENNETH H. LENERS, Captain, USAF
Project Manager
Directorate of Technology

Approved for publication:

FOR THE COMMANDER

MARION L. LASTER
Director of Technology
Deputy for Operations

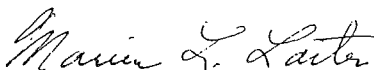| REPORT DOCUMENTATION PAGE		READ INSTRUCTIONS BEFORE COMPLETING FORM
1. REPORT NUMBER AEDC-TR-79-88	2. GOVT ACCESSION NO.	3. RECIPIENT'S CATALOG NUMBER
4. TITLE (and Subtitle) LASER-RAMAN FLOW-FIELD DIAGNOSTICS OF TWO LARGE HYPERSONIC TEST FACILITIES		5. TYPE OF REPORT & PERIOD COVERED Final Report, April 13, 1977 - July 10, 1978
		6. PERFORMING ORG. REPORT NUMBER
7. AUTHOR(s) W. D. Williams, D. A. Wagner, H. M. Powell, and L. L. Price, ARO, Inc., a Sverdrup Corporation Company		8. CONTRACT OR GRANT NUMBER(s)
9. PERFORMING ORGANIZATION NAME AND ADDRESS Arnold Engineering Development Center/DOT Air Force Systems Command Arnold Air Force Station, Tennessee 37389		10. PROGRAM ELEMENT, PROJECT, TASK AREA & WORK UNIT NUMBERS Program Element 65807F
11. CONTROLLING OFFICE NAME AND ADDRESS Arnold Engineering Development Center/DOS Arnold Air Force Station, Tennessee 37389		12. REPORT DATE December 1979
		13. NUMBER OF PAGES 38
14. MONITORING AGENCY NAME & ADDRESS(if different from Controlling Office)		15. SECURITY CLASS. (of this report) UNCLASSIFIED
		15a. DECLASSIFICATION/DOWNGRADING SCHEDULE N/A

16. DISTRIBUTION STATEMENT (of this Report)

Approved for public release; distribution unlimited.

17. DISTRIBUTION STATEMENT (of the abstract entered in Block 20, if different from Report)

18. SUPPLEMENTARY NOTES

19. KEY WORDS (Continue on reverse side if necessary and identify by block number)

lasers	temperature	nonequilibrium flow
Raman spectra	free stream	
scattering	excitation	
flow fields	molecules	
hypersonic wind tunnels	Mach numbers	

20. ABSTRACT (Continue on reverse side if necessary and identify by block number)

Laser-Raman scattering has been utilized to discover nonequilibrium N_2 vibrational levels in a continuous, resistance-heated wind tunnel (Tunnel C) and in an arc-heated wind tunnel (Tunnel F). Vibrational temperatures of up to two times the bulk reservoir temperature have been measured in the Tunnel F free stream. A double-diaphragm device for delay of the Tunnel F nozzle expansion was found to significantly reduce the vibrational temperature

DD $_{1\ JAN\ 73}^{FORM}$ 1473   EDITION OF 1 NOV 65 IS OBSOLETE

20. ABSTRACT (Continued)

level. In Tunnel C, the vibrational temperatures were found to be dependent upon the water vapor concentration in the flow. It is hypothesized that water vapor-induced de-excitation of the vibrationally excited nitrogen molecules results in a significant rise in local static temperature and corresponding reduction in Mach number.

AFSC
Arnold AFS Tenn

PREFACE

The work reported herein was conducted by the Arnold Engineering Development Center (AEDC), Air Force Systems Command (AFSC), and the Air Force project manager was Capt. Stanislaus L. Ludwig (CF). The results of the research were obtained by ARO, Inc., AEDC Division (a Sverdrup Corporation Company), operating contractor for the AEDC, AFSC, Arnold Air Force Station, Tennessee, under ARO Project No. P32M-01. The data analysis was completed on September 30, 1978, and the manuscript was submitted for publication on October 17, 1979.

CONTENTS

ILLUSTRATIONS

TABLES

1.0 INTRODUCTION

1.1 PURPOSE OF THE MEASUREMENTS

As early as 1966, electron beam fluorescence measurements of the static temperature (T_∞) of the von Kármán Gas Dynamics Facility (VKF) Hypervelocity Wind Tunnel (F) at the Arnold Engineering Development Center (AEDC) revealed a significant discrepancy between measured values and those derived from utilizing pressure and heat-transfer measurements. Unfortunately, the electron beam technique had not reached its present confidence level (Refs. 1 and 2), and the measurements were, for the most part, dismissed.

In 1969 pressure measurements on flat plates and cones indicated that the free-stream properties obtained for the VKF Hypersonic Wind Tunnel (C) might be incorrect. As a result of the continued experimentation and improved confidence in electron beam diagnostics, it was decided to measure the static temperature in VKF Tunnel C using the electron beam fluorescence technique. The results of the measurements showed a dependence upon the humidity level of the flow field. At dewpoints approaching -60°F (-51°C) the measured temperatures were in agreement with static temperature predictions based on three different methods. However, as the dewpoint was increased to -30°F (-23°C) the deviation between the measured and pressure-derived values was as much as +25°K for the case where the static temperature for a -60°F dewpoint was $\approx 50°K$.

The temperature values determined by gas-dynamic (or pressure) measurements are, of course, secondary parameters in the sense that static and dynamic pressure measurements are used to determine the flow-field Mach number, M, and from the Mach number the static temperature is obtained. Clearly, several assumptions are required to effect a gas-dynamic temperature measurement and primary among these assumptions is the assertion that the flow-field expansion is isentropic. The pressure measurements which had been used for obtaining the flow-field Mach number and free-stream temperature included impact, or pitot, probe measurements, for which the ratios of the impact pressure (p_o') and either the reservoir pressure (p_o) or the static pressure (p_n) at the nozzle wall were determined. Also, pressure measurements were obtained using a blunt cone which was located within the flow field. Regarding the blunt cone measurement, the ratio of the impact pressure (p_o') of the cone and the surface pressure (p_c) on the cone, which was corrected for viscous flow effects, were formed to yield a local flow-field Mach number. Designating the Mach numbers M_1, M_2, and M_3 to be those values determined by the ratios p_o'/p_o, p_o'/p_n, and p_o'/p_c, respectively, it was found that $M_1 \approx M_2 \approx M_3$ for a dewpoint of -60°F. Further, the static temperatures $T_{1,2, \text{ and } 3}$ corresponding to $M_{1,2, \text{ and } 3}$ agreed with the local value T_∞ provided

by the electron beam measurement. However, as the dewpoint increased from -60°F to -30°F discrepancies between the various temperatures appeared and increased with increasing dewpoint.

Quantitatively, the Mach number discrepancy can be summarized as follows:

a. Three standard methods for Mach number measurement give three different Mach numbers for specific humidity levels greater than about 10^{-5}.

b. The most reliable Mach number, M_3, was observed to decrease ten percent as specific humidity increased from 1.9×10^{-5} to 2×10^{-4} grams of water per gram of dry air.

c. Electron beam measurements of static temperature yielded temperature values ≈ 50 percent higher than predicted from M_1 and ≈ 30 percent higher than predicted from M_3 at the highest humidity level.

d. At a dewpoint level of -60°F the predicted values of static temperature based on M_1, M_2, and M_3 agreed with the electron beam values.

e. Ar, H_2O, and CO_2 condensation in the flow field could increase static temperature less than five percent at a Mach number = 10 condition.

Interest in the Mach number ambiguity was renewed in 1976 when an apparently similar process was discovered in the AEDC VKF Tunnel F. The hypothesis was advanced that de-excitation of the nitrogen vibrational energy mode in the downstream portion of the nozzle flow field could account for the observed phenomena. Classical nonequilibrium calculations indicated that sufficient energy for driving the heat addition (diabatic) process would be available from nonequilibrium or "frozen" N_2 vibrational levels. However, neither experimental measurement of the vibrational nonequilibrium nor any information on a possible mode of deactivation was available.

The objectives of this investigation were to determine if, indeed, vibrational nonequilibrium existed and upon what flow parameters did the degree of nonequilibrium depend.

1.2 LASER-RAMAN DIAGNOSTIC TECHNIQUE

In order to investigate the degree of vibrational nonequilibrium in the hypersonic flow field of interest, a noninterfering, nonobtrusive diagnostic technique was needed. The laser-

Raman scattering technique had been developed at AEDC and utilized for the study of condensation phenomena in the supersonic/hypersonic flow fields of various small nozzles (Refs. 3 and 4). In these studies, static temperature of the gases had been inferred from measurements of the rotational temperature; also, heat addition to the flow, as a result of homogeneous condensation processes, had been detected. Because the reliability and noninterference of the technique had been sufficiently demonstrated, it was decided to utilize laser-Raman scattering for the continued investigation of the Mach number problem.

Laser-Raman scattering (Refs. 5 and 6) results from the inelastic interaction between laser beam photons and flow-field molecules. This interaction produces molecular energy level transitions, and, subsequently, scattered radiation at wavelengths specific to the gas molecule and energy level transition. The Raman vibration-rotation spectrum of N_2 is of particular interest here because of the high concentration of N_2 in the flows of VKF Tunnels F and C and the interest in the N_2 vibrational nonequilibrium. Computer-generated synthetic vibration-rotation spectra of N_2 are shown in Figs. 1 through 4. The spectra shown in Figs. 1 through 4 were calculated for a 0.85-m double spectrometer with 1,200 g/mm gratings and 2-mm wide slits giving a spectral dispersion of $\approx 4.5 \, \text{Å}/\text{mm}$. A triangular slit function was used for the spectral convolution, and Fig. 5 shows the agreement between
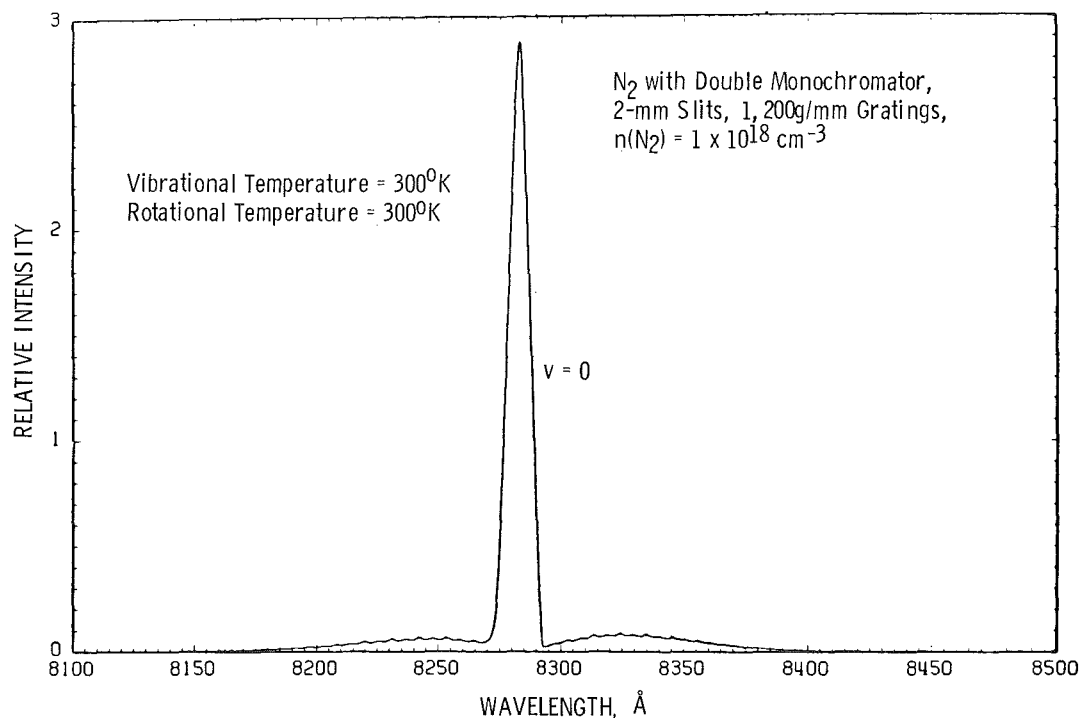
Figure 1. N_2 vibration-rotation band at room temperature equilibrium conditions.

measured and calculated profiles of the N_2 vibration-rotation band at room temperature atmospheric conditions. Figure 1 shows the spectrum at room temperature, equilibrium conditions, and Figs. 2 through 4 show the spectrum for high degrees of nonequilibrium between the rotational and vibrational modes. As a result of molecular anharmonicity, the contributions to the spectrum from the N_2 vibrational levels are easily separable with only moderate spectral dispersion.

The ratio of the intensity (R) of the $v = 1$ and $v = 0$ peaks, defined by

$$R = I (v = 1) / I (v = 0) \qquad (1)$$

is a function of temperature. This intensity ratio is plotted as a function of T_v in Fig. 6. For the static or rotational temperature range of 50 to 150°K expected for VKF Tunnels F and C, the ratio is independent of rotational temperature. Therefore, a simultaneous measurement of the intensities $I(v = 1)$ and $I(v = 0)$ and the predicted intensity ratio curve can give a determination of T_v in the flow field.
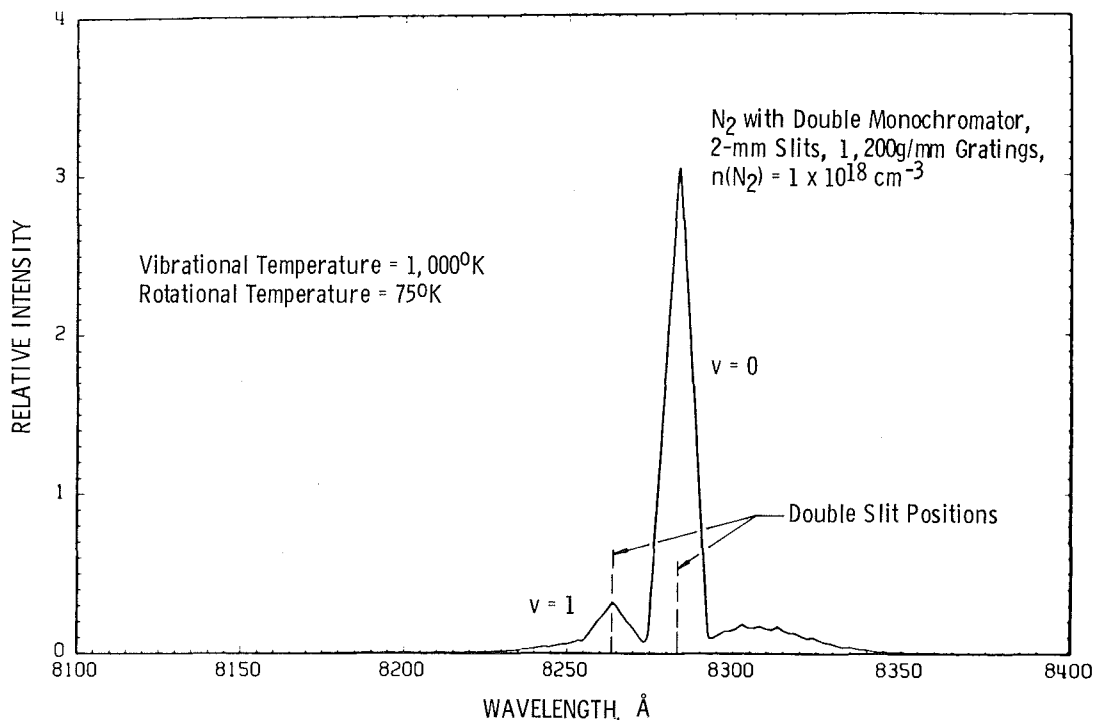
Figure 2. N_2 vibration-rotation band at T_v = 1,000°K, T_R = 75°K.
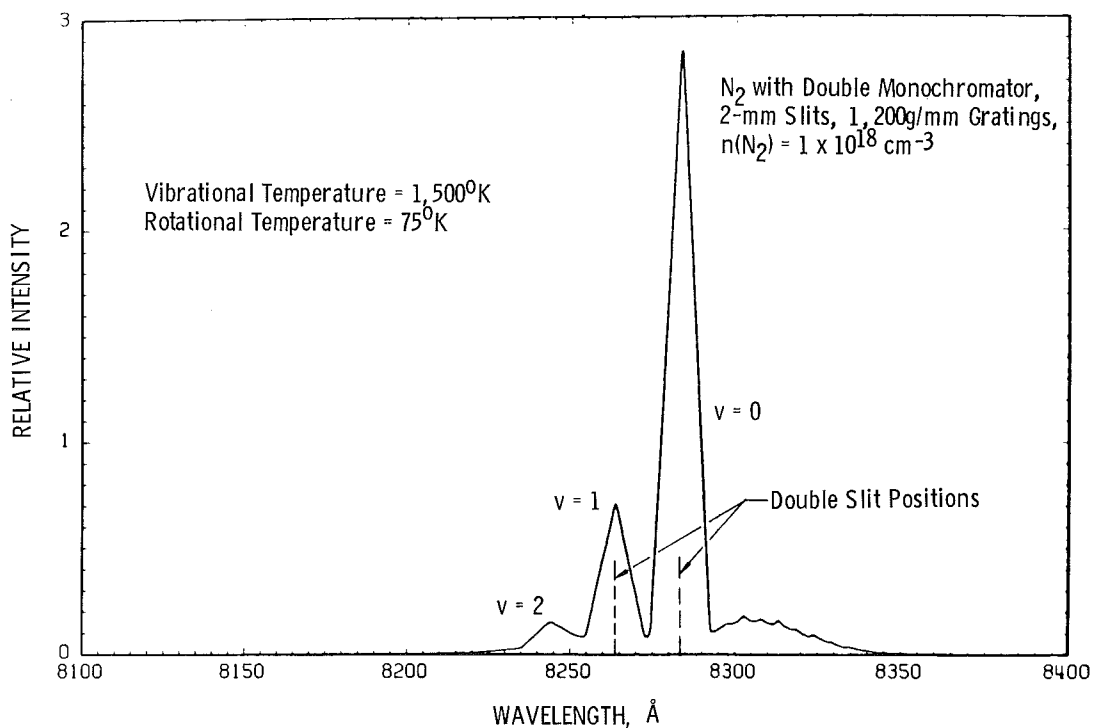
Figure 3. N_2 vibration-rotation band at T_v = 1,500° K, T_R = 75° K.
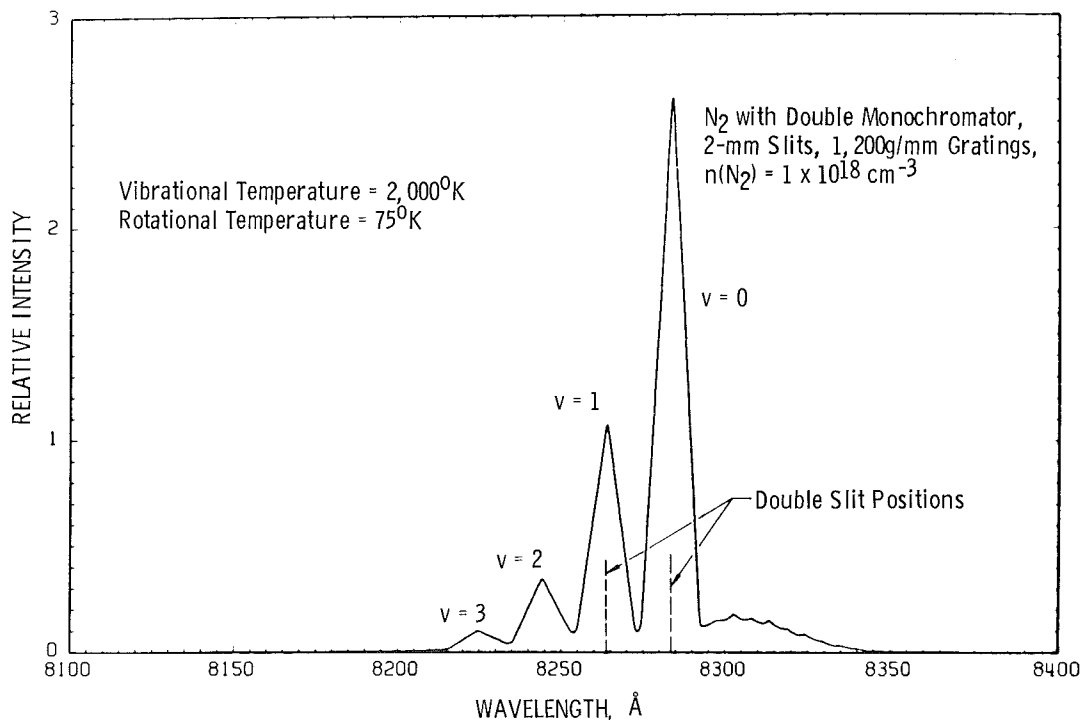
Figure 4. N_2 vibration-rotation band at T_v = 2,000° K, T_R = 75° K.

9
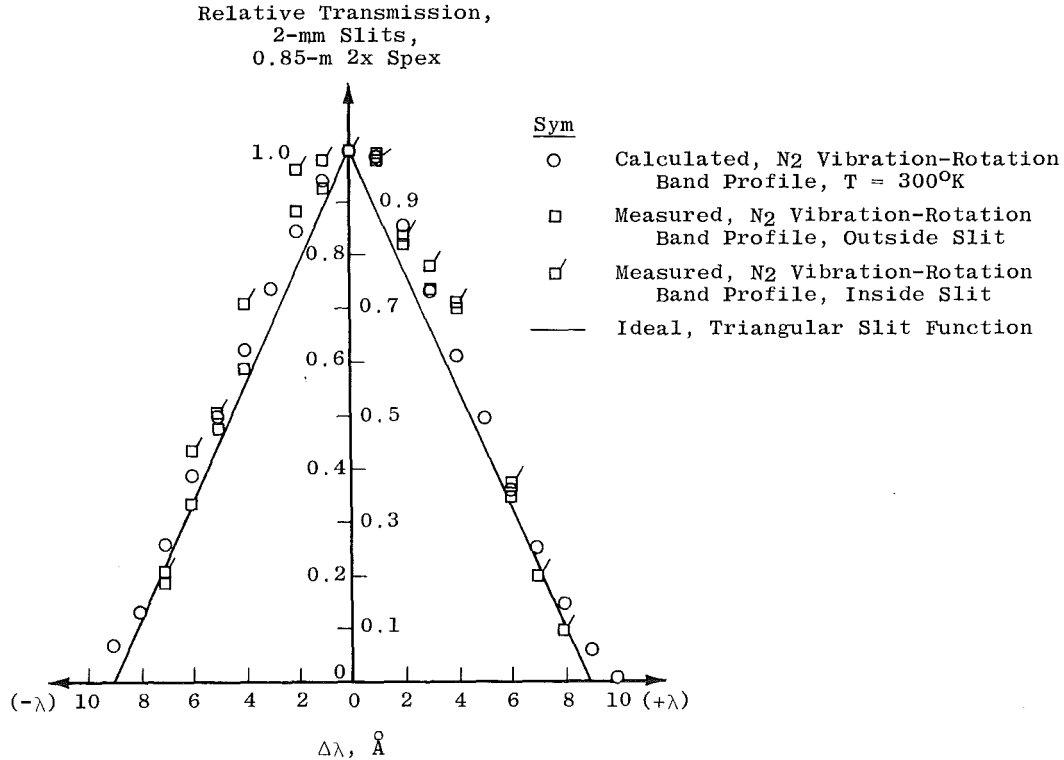
Figure 5. Spectrometer transmission function.

The intensity of the N_2 vibration-rotation band is directly proportional to the N_2 number density, $n(N_2)$. Therefore, $n(N_2)$ can also be determined simultaneously with a T_v measurement using the relation

$$n(N_2) = C_{F_2} I_m (v = 0) C_{F_1} \qquad (2)$$

C_{F_1} is a calibration factor determined at room temperature atmospheric conditions, and C_{F_2} is a calculated temperature-dependent factor plotted in Fig. 6.

1.3 DESCRIPTION OF THE FLOW FIELDS INVESTIGATED

The VKF Tunnel F is a large, arc-heated blowdown wind tunnel (Hotshot Tunnel), and the Tunnel F plant is shown in Fig. 7. The tunnel is operated with dry nitrogen as the test gas. Before each run the arc chamber, which serves as the tunnel reservoir, is purged with dry nitrogen to eliminate atmospheric oxygen and water vapor. The chamber is then charged to some initial pressure which may range from a few hundred psia (≈ 14 atm) up to 20,000 psia (1.4×10^3 atm) depending on the desired test conditions. Energy, previously stored in a 280-μh inductance coil with a rating of 60 MJ, is then added to the gas by means of arc
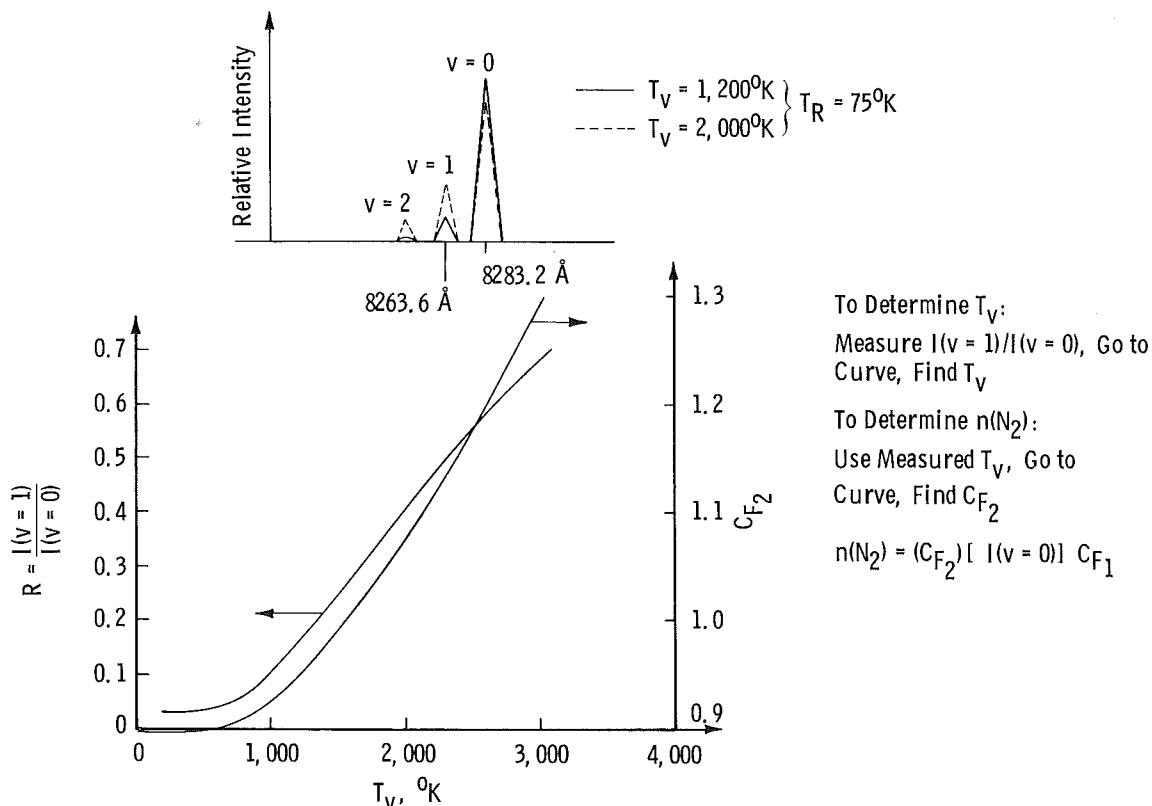
Figure 6. Intensity ratio, R, and temperature-dependent parameter C_{F_2} as functions of vibrational temperature for $50°K \leqslant T_R \leqslant 150°K$.

discharge. Initial arc current may vary from 100,000 to 600,000 A depending on the quantity of energy stored in the coil. Approximately 50 percent of the coil energy is delivered to the test gas by the arc heating process. The total arc discharge time varies from 10 to 70 msec depending on the initial charge pressure and coil energy. The pressure rise during arc discharge causes a single diaphragm separating the arc chamber from the tunnel nozzle to rupture, and flow starts in the nozzle. The tunnel can also be operated with a double-diaphragm apparatus which delays the start of flow in the nozzle for some predetermined time after arc discharge. The added delay allows more time for additional mixing of the arc-heated gas with the cooler surrounding gas.

The Tunnel F nozzles consist of a family of three axisymmetric, contoured nozzles designed to operate at Mach numbers of 8, 12, and 16. These nozzles have exit diameters of 25 in. (63.5 cm), 40 in. (1.02 m), and 48 in. (1.22 m); throat diameters of 1.875 in. (4.76 cm), 1.063 in. (2.70 cm), and 0.609 in. (1.55 cm); and expansion sections with half angles of 4, 7, and 10 deg, respectively.

11

The VKF Tunnel C (Fig. 8) is a closed-circuit, hypersonic wind tunnel with a Mach 10 axisymmetric contoured nozzle and a 50-in. (1.27 m)-diam test section. The throat diameter is 1.746 in. (4.435 cm), and the nozzle length from the throat to the test section entrance is 295 in. (7.49 m). Just downstream of the throat, the nozzle is very nearly conical with a half-angle of approximately 9 deg. This section of the nozzle generates a spherical source flow which is then turned parallel to the nozzle axis by the contoured section of the nozzle.
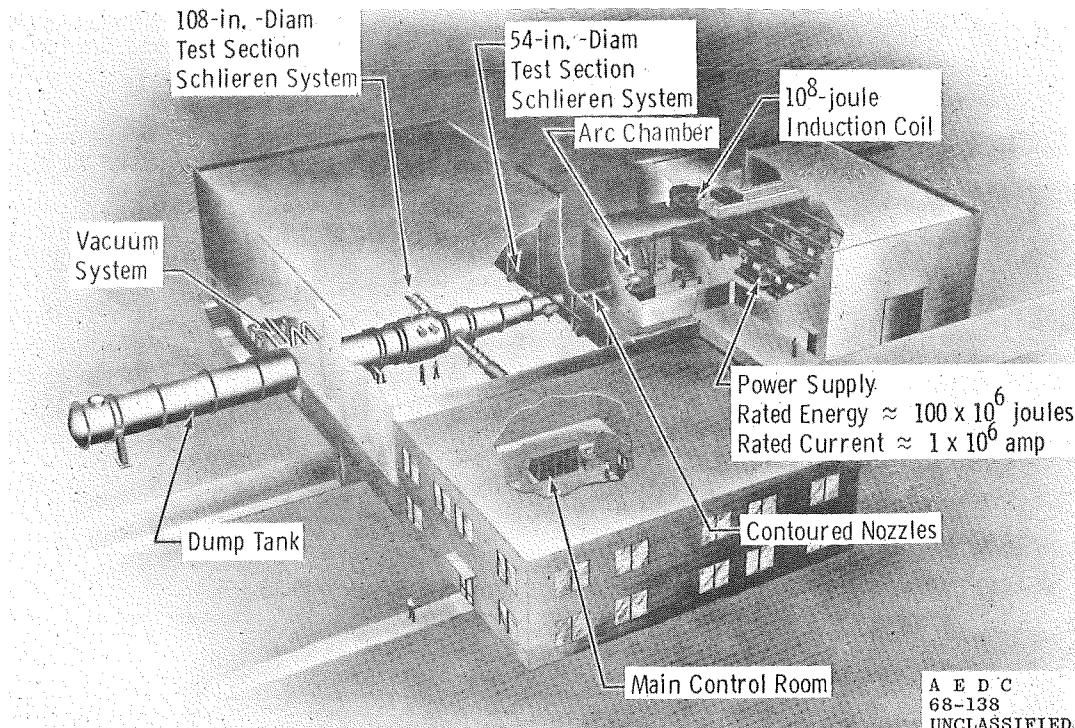
Figure 7. AEDC-VKF Tunnel F.

The tunnel can be operated continuously over a stagnation pressure range from 200 psia (13.5 atm) to 2,000 (136 atm) psia with air supplied by the VKF main compressor plant. Stagnation temperatures up to 1,200°K are obtained through the use of a natural gas-fired combustion heater in series with an electric resistance heater. The moisture content of the test air is controlled by a vertical, deep bed drier which contains approximately 13,500 lb (6,129 kg) of beaded (spherical) silica-gel with an average bead diameter of 0.138 in. (0.351 cm). For normal operation the stagnation temperature is set at 1,055°K, and the air specific humidity is kept below 10^{-5}.

TEST SECTION

INSTRUMENTATION RING

QUARTZ WINDOWS

MODEL SUPPORT
INJECTION/RETRACTION
SYSTEM

SCREEN
SECTION

THROAT
SECTION

NOZZLE

SAFETY DOOR

DIFFUSER SECTION

TRANSITION
SECTION

WATER
FLOW

FAIRING
DOOR

TANK
ENTRANCE
DOOR

MODEL COOLING
AIR LINE

PRESSURE TRANSDUCER
SYSTEM

OPERATION
FLOOR

MODEL COOLING
NOZZLES

TEST SECTION TANK

FEET

a. Tunnel assembly

WINDOWS FOR MODEL INSPECTION
OR PHOTOGRAPHY

WINDOWS FOR SHADOWGRAPH/
SCHLIEREN PHOTOGRAPHY

AIR DUCTS TO COOL
MODEL FOR HEAT-
TRANSFER TESTS OR
QUICK MODEL CHANGE

PRESSURE TRANSDUCERS
AND VALVES

NOZZLE

TANK ENTRANCE DOOR
FOR MODEL INSTALLATION
OR INSPECTION

MODEL INJECTION AND
PITCH MECHANISM

b. Tunnel test section
Figure 8. AEDC-VKF Tunnel C.

13

2.0 EXPERIMENTAL SETUP AND OPERATION AT TUNNEL F

2.1 OPTICAL SYSTEM

Laser-Raman measurements were made at both the 54-in. (1.37 m)-diam (upstream) and ablation test sections of Tunnel F. The setup at the 54-in. (1.37 m)-diam test section is shown schematically in Fig. 9 and photographically in Fig. 10. The laser system, spectrometer, and collection optics were all mounted on a large metal baseplate; and this baseplate was secured to a vibration-isolation stand (see Fig. 10) that was normally used to hold one of the
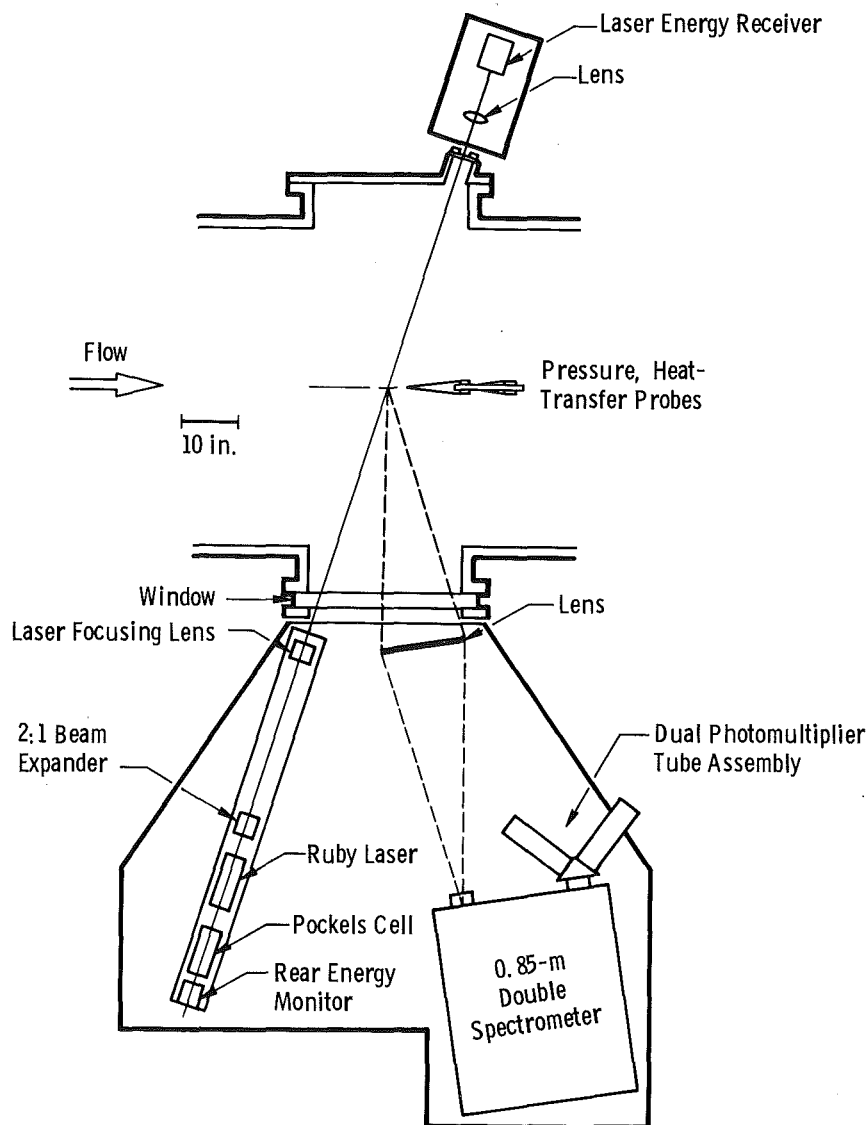
Figure 9. Experimental setup at Tunnel F 54-in. test section.

schlieren system mirrors at the 108-in. (2.74 m)-diam (downstream) test section. The Q-switched, amplified ruby laser system was focused on the axial centerline of Tunnel F and the laser could deliver four to six joules per pulse on the centerline at a wavelength of 6943 Å. Raman scattered radiation was collected from the beam focal volume by a Fresnel lens and imaged through a high-pass optical filter onto the entrance slit of the spectrometer. A Spex 0.85-m double spectrometer with 1,200 g/mm gratings was utilized, and it was equipped with a double exit slit assembly to provide simultaneous signals at the v = 0 and v = 1 spectral locations. The radiation transmitted through the slits was detected by a pair of RCA-C31034A photomultiplier tubes (PMT).
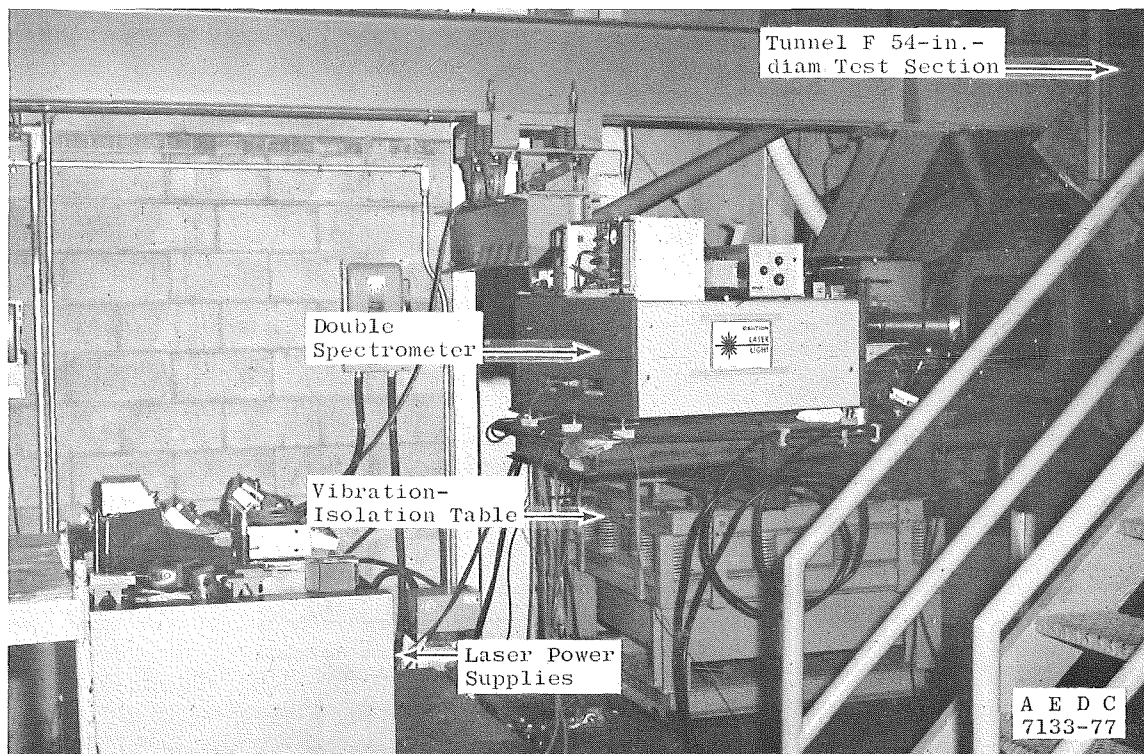
Figure 10. Photograph of installation at Tunnel F 54-in. test section.

As shown in Fig. 9, an energy meter was mounted on a stand opposite the laser input position to measure the laser beam transmission was well as to trap the beam for safety purposes. The energy meter was of the calorimetric type with a slow response time; therefore, its output could be recorded with a strip chart. The laser input energy, as well as pulse shape, was monitored with a photomultiplier/filter assembly at the rear of the laser.

The setup at the ablation test section near the arc chamber (see Fig. 7) is shown schematically in Fig. 11. The ruby laser system was positioned directly above the double spectrometer input side by use of an aluminum table secured to the top of the vibration-isolation mount. The laser beam was not amplified or focused for the ablation test section measurements to avoid possible gas breakdown as a result of high gas densities and optical power density. The laser beam was deflected down and across the center of the test section with a mirror. The laser beam receiver, collection optics, spectrometer, and detectors were the same as used for the measurements at the 54-in.-diam test section.
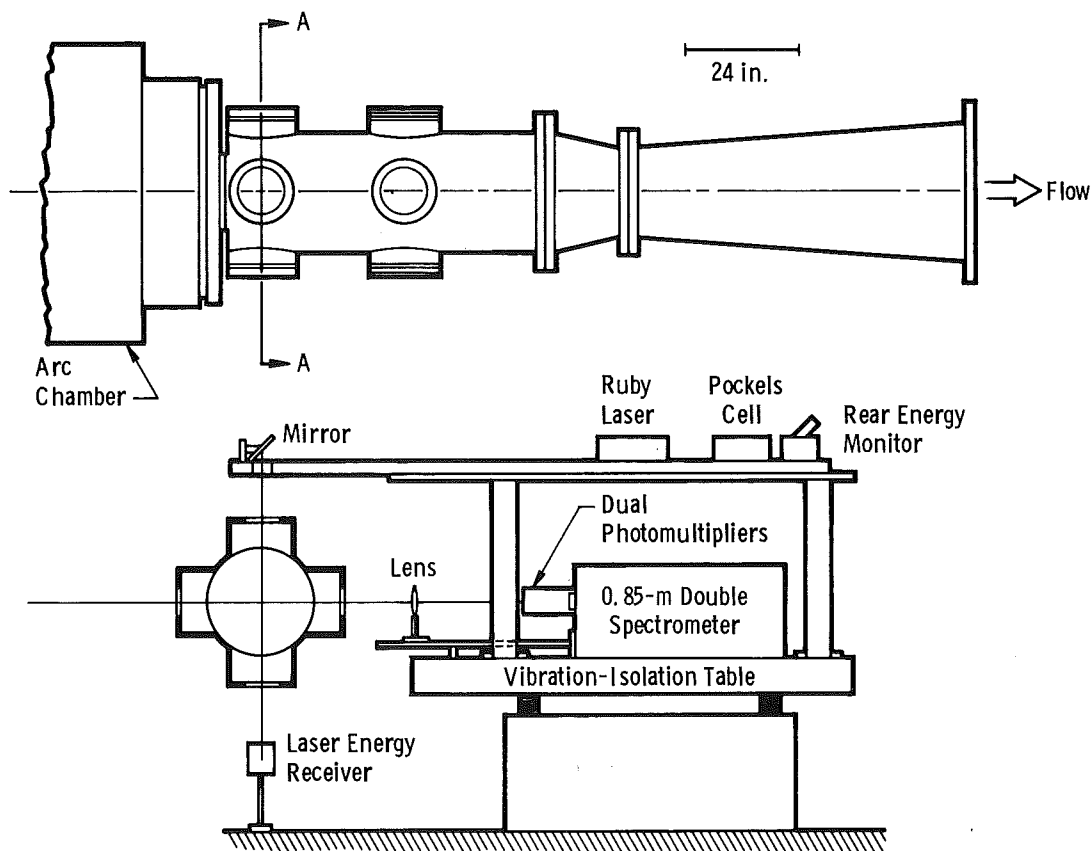
Figure 11. Experimental setup at Tunnel F ablation test section.

2.2 DATA ACQUISITION

The significant features of the data acquisition functions concern the timing, tunnel synchronization, laser control, and data readout features. The technique for acquiring the data has been reported elsewhere (Ref. 7) and basically involves recording the PMT outputs on a fast-storage oscilloscope. The oscilloscope display is subsequently scanned by a vidicon

system under processor control such that the display is retained in memory for data reduction purposes. The composite system thus involved control and synchronization with the tunnel operation of this transient recording technique and the laser light injection devices. A photograph of data acquisition instrumentation is presented in Fig. 12.
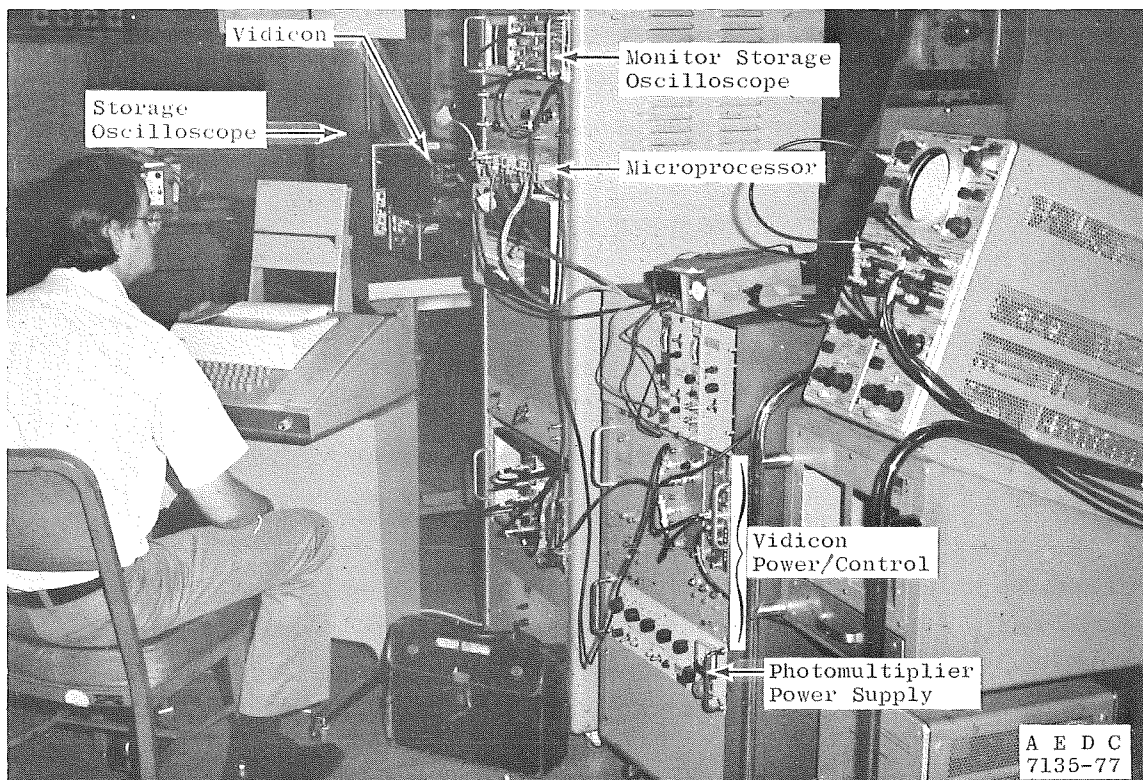
Figure 12. Photograph of data acquisition instrumentation
for Tunnel F measurements.

The actual recorded input data as retained in memory appears as a series of numbers according to memory address whose magnitude is proportional to oscilloscope display position above some arbitrary baseline. There is a one-to-one relationship between memory address and the horizontal position of each display resolution element. The ultimate tabulated output is the summation of those numbers representing those display elements defining the PMT waveform of interest. The respective PMT waveforms are displaced temporally by insertion of an additional coaxial line which in effect introduces additional delay. Thus the transient waveform for each PMT is defined by the contents of a segment of memory. The storage oscilloscope display was defined by 256 x 256 elements in both horizontal and vertical direction. Additional details of the technique can be obtained from the references noted above.

The usual procedure of performing a background and data measurement was applicable as in other similar situations. The background measurement preceded a scattering data measurement while the tunnel was evacuated, approximately 25 sec before diaphragm rupture. Both scattering and background data were read into the processor in the same fashion. A data acquisition cycle includes the following sequence:

1. Vidicon Target Preparation

2. Laser Charge

3. Oscilloscope Reset

4. Function Synchronization Selection

5. Variable Delay "Time-Out"

6. Laser Status Check

7. Laser Fire

8. Data Input from Storage Oscilloscope to Processor Memory

9. Data Display from Processor Memory to Display Oscilloscope

The synchronization selection noted in Item 4 functions in a manual or tunnel select mode, the former being the background measurement and the latter being the Raman scattering measurement. The sequences are identical for the background and data measurements otherwise, with the exception of the processor memory location of the data for the respective measurements. The delay "time-out" is for the purpose of adjusting the instant of data acquisition relative to the instant of arc time. After data acquisition was completed a correction for the background component of the signal was made, and the intensity of each PMT input was determined by summation of the values stored in assigned memory location corresponding to each PMT temporal display. Subsequently, temperature and density values were determined using the results of this summation process.

2.3 CALIBRATIONS AND DATA REDUCTION

Calibrations were made before each tunnel firing with the tunnel opened to the atmosphere. Atmospheric pressure, temperature, and relative humidity were recorded and used to calculate the dry air number density. A nitrogen mole fraction of 0.7808 was assumed. The calibration constant C_{F_1} of Eq. (2) was determined from

$$C_{F_1} = n^\circ(N_2)/T_F^\circ I_m^\circ(v=0) \tag{3}$$

in which

$$T_F^o = \frac{2\ E_{vac}}{E^o + E_{vac}} \tag{4}$$

E_{vac} is the transmitted laser energy when the tunnel was evacuated, and E^o is the transmitted laser energy when the tunnel was open to atmospheric pressure.

The relative sensitivity of the detectors (R_R) was determined by adjusting the spectrometer wavelength dial to place the $v = 0$ signal on one detector and then on the other. A measured intensity ratio for a tunnel firing was then determined by

$$R = \left[\frac{I_m^t\ (v = 1)}{I_m^t\ (v = 0)}\right] R_R \tag{5}$$

and T_v was then graphically determined from Fig. 6.

Using the measured value of T_v, a C_{F_2} value was graphically determined from Fig. 6. The measured N_2 number density was then determined from

$$n_m\ (N_2) = C_{F_2}\ I_m^t (v = 0)\ C_{F_1}\ T_F^t \tag{6}$$

in which

$$T_F^t = \frac{2\ E_{vac}}{E^t + E_{vac}} \tag{7}$$

E^t is the transmitted laser energy during a tunnel firing.

3.0 EXPERIMENTAL SETUP AND OPERATION AT TUNNEL C

3.1 OPTICAL SYSTEM

The experimental arrangement for the Tunnel C measurements is shown schematically in Fig. 13 and photographically in Fig. 14. The laser system, spectrometer, and collection optics were mounted in a stacked arrangement. The entire assembly was mounted on the vibration-isolation support normally used to hold a portion of the schlieren system. The conventional mode, amplified ruby laser system was focused near the axial centerline of the tunnel, and the system could deliver 70 joules per pulse to the focal volume. A conventional

Cross-Sectional
View of Test Section
(Looking Downstream)

1.	Test Section	8.	0.85-m Double
2.	Ruby Laser		Spectrometer
3.	Beam Expander	9.	Photomultiplier and
4.	Mirror		Cooler
5.	Quartz Window	10.	Fresnel Lens
6.	Focused Laser Beam	11.	Vibrational Isolation
7.	Pyroelectric Detector		Support
		12.	Rigid Diagnostic Table
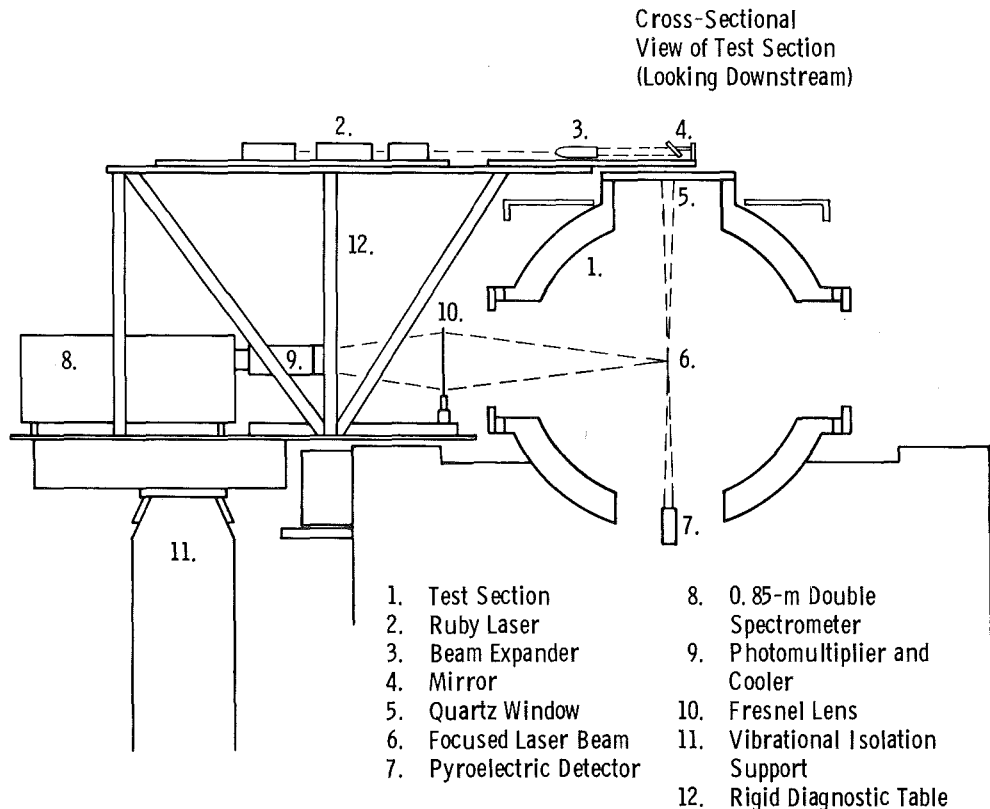
Figure 13. Raman scattering experimental setup at Tunnel C.

mode laser was chosen because it could deliver an order of magnitude more energy per pulse to compensate for the nearly order of magnitude drop in number density between the Tunnels F and C flow fields. The collection optics, spectrometer, double slit assembly, and photomultipliers were the same as used for the Tunnel F measurements. The detectors were, however, maintained at -26°C by thermoelectric coolers to reduce dark current.

A pyroelectric detector was mounted in the tank below the test section to measure laser energy transmission and to trap the beam. Laser input energy was determined with the same monitor system as used for the Tunnel F measurements.

3.2 DATA ACQUISITION

As noted elsewhere, photon counting techniques were utilized for the light scattering measurements in Tunnel C. A minicomputer-controlled automatic data acquisition system, which has been documented elsewhere (Ref. 7), was used in this study. In fact, Ref. 7 provides most of the details of the hardware features of the system. However, certain new

software features were implemented for the Tunnel C measurements, and these included new calibration and data reduction additions.
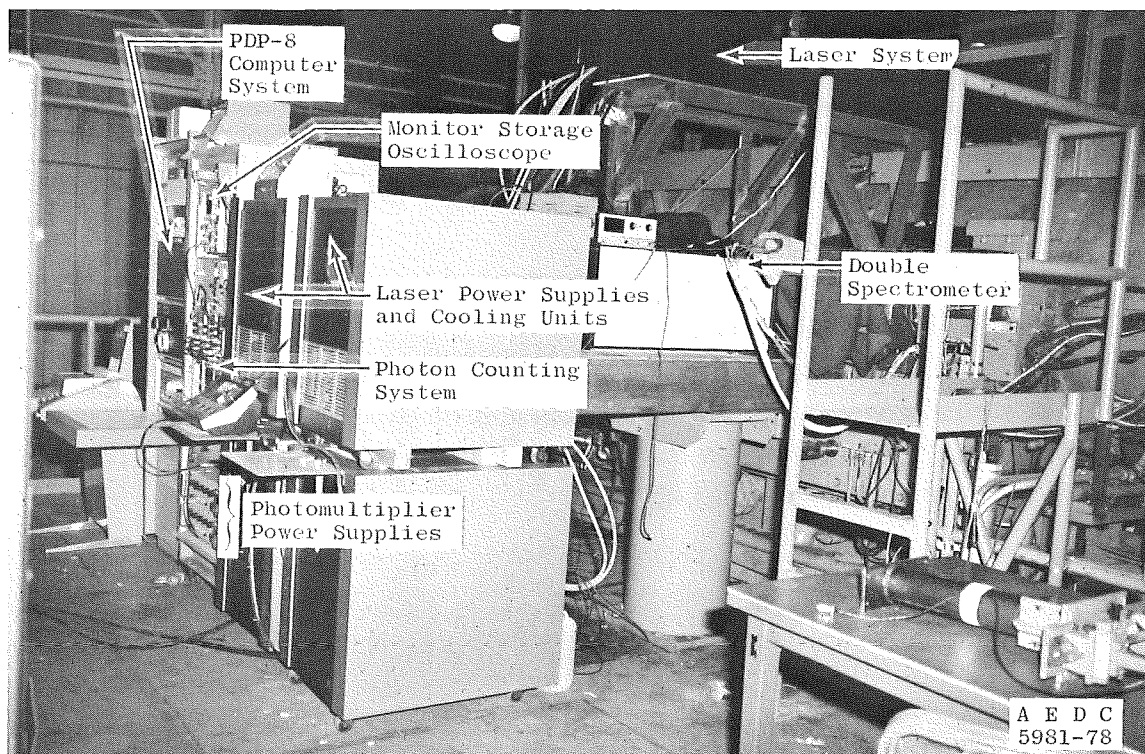
Figure 14. Photograph of instrumentation at Tunnel C.

The most notable difference between the system of current interest and previous systems is the amplified laser configuration. Obviously, the charging of both the oscillator and amplifier system must be properly synchronized and the subsequent flash-lamp ignition properly timed for optimum laser performance. The ready flag of each laser was input to the processor through a digital input buffer. When both were in a ready situation, the program generated a laser fire pulse. The appropriate timing relative to the respective flash lamps was provided in the laser interface. This system provided the required delay between the two flash-lamp ignitions for optimum output.

Additionally, a pyroelectric energy meter with provision for direct or remote signal measurement was also included in these measurements.

21

3.3 CALIBRATIONS AND DATA REDUCTION

Initial calibrations at Tunnel C required determination of the photon counting dead time (Ref. 8) for each detector channel. The spectrometer wavelength dial was separately adjusted such that the variation of I(v = o) with laser energy could be determined by each detector. As shown in Ref. 8 for a nonparalyzable photon counting system

$$\frac{E^\circ}{I_m{}' (v = 0) \, / \, \tau_g} = E^\circ \tau_D + C \tag{8}$$

where C is a constant, E° is the laser energy, $I_m{}'(v = 0)$ is the detected intensity in photon counts, τ_g is the photon counting interval, and τ_D is the detector channel dead time. Therefore, a plot of $E^\circ \tau_g / I_m{}'(v = 0)$ as a function of E° gives a straight line, the slope of which yields τ_D. Typical dead times for the detector channels were 40 nsec. Correction of intensity values are then made using the relation

$$I_m (v = 0) = \frac{I_m{}' (v = 0)}{1 - I_m{}' (v = 0) \, (\tau_D \, / \tau_g)} \tag{9}$$

Determination of the density calibration constant, C_{F_l}, and relative sensitivity of the detector channels, R_R, used the same relations as used for Tunnel F calibrations. However, for Tunnel C calibrations the laser was fired 50 times for each calibration value, and numerical averaging was used to determine intensity and energy values.

Data reduction also used the same relations as for Tunnel F, and again, numerical averaging over 50 laser pulses was used to determine intensity and energy values.

4.0 DISCUSSION OF RESULTS

4.1 PRESENTATION OF DATA

A series of N_2 vibrational temperatures and number density measurements were conducted in Tunnel F in the Mach 8 contoured nozzle at a point 377 in. (9.58 m) downstream of the throat and in the Mach 12 contoured nozzle at points located 32 in. (0.81 m) and 379 in. (9.63 m) downstream of the throat. Runs were made with both single- and double-diaphragm sections in order to determine the effect of delay time on vibrational temperature and Mach number. The results of these experiments are summarized in Table 1.

Table 1. Tunnel F Parameters, Measured and Calculated

Run	Nozzle	Diaphragm	$\Delta\tau$, msec	t, msec	p_o, psia	T_o, °K	p_∞, psia	T_∞, °K	$n_c(N_2)$, cm^{-3}	M_3	M_1	T_v, °K	$n_m(N_2)$, cm^{-3}	$S(T_v)$, percent	$u(T_v)$, percent	$S(n_m)$, percent	$u(n_m)$, percent
					Tunnel Conditions Calculation							Laser–Raman System					
5,700	M 8 (Sta 390)	Single	~0	130	4,228	898	0.722	88.0	4.10×10^{18}	6.99	7.71	1,850	5.6×10^{18}	5.6	14	3.6	11
5,701		Single	~0	110	5,102	858	0.857	81.0	5.29×10^{18}	7.11	7.74	2,130	8.4×10^{18}	5.1	13	3.1	10
5,706		Single	~0	110	5,162	876	0.891	83.4	5.32×10^{18}	7.07	7.71	1,650	8.3×10^{18}	5.6	14	3.6	11
5,707		Double	463	112	~5,526	608	0.637	49.7	6.41×10^{18}	7.59	—	<500	5.7×10^{18}	7.7	18	3.1	10
5,713	M 12 (Sta 390)	Single	~0	130	9,086	1,416	0.101	64.7	7.81×10^{17}	10.82	11.43	2,150	1.3×10^{18}	15.3	33	6.6	17
5,712		Double	628	130	7,306	1,281	0.0946	75.7	6.25×10^{17}	9.38	11.78	1,100	8.95×10^{17}	17.3	37	6.1	16
5,795	M 12 (Sta 390)	Single	~0	114	10,967	1,577	0.119	77.1	7.72×10^{17}	10.53	11.63	2,800	1.3×10^{18}	11.2	25	7.1	18
5,798		Single	~0	112	10,660	1,641	0.119	77.6	7.70×10^{17}	10.72	11.42	—	—	—	—	—	—
5,796		Double	329	112	9,866	1,424	0.116	79.5	7.30×10^{17}	9.76	11.77	1,950	6.6×10^{17}	8.2	19	5.6	15
5,797		Double	436	112	9,694	1,392	0.109	77.0	7.08×10^{17}	9.79	11.88	1,800	5.34×10^{17}	7.7	18	4.6	13
5,801	M 12 (Sta 43)	Single	~0	137	—	—	—	—	—	—	—	3,000	3.1×10^{19}	6.1	15	5.6	15
5,802		Double	217	129	—	—	—	—	—	—	—	1,700	1.1×10^{19}	14.8	32	11.2	26
5,803			447	127	—	—	—	—	—	—	—	1,750	1.7×10^{19}	13.3	29	8.4	20
5,804			647	126	—	—	—	—	—	—	—	—	—	—	—	—

The Tunnel C experiments were run at a reservoir pressure and temperature of 1,470 psia (100 atm) and 1,200°K, respectively. At this temperature, the nitrogen vibrational energy states contain approximately 50 percent more energy than at the standard reservoir temperature of 1,055°K. The air frost-point temperature was the primary flow variable and was controlled over the extreme limits of -10°C to -55°C by the VKF plant driers. This range corresponds to specific humidity, ω, ranging from 1.6×10^{-3} down to 1.3×10^{-5} g H_2O/g dry air. N_2 vibrational temperature and number density were monitored by the laser-Raman system, and the results are summarized in Table 2.

In both Tables 1 and 2 imprecision (random error) numbers are assigned to each of the values measured by the laser-Raman system. These numbers were calculated using the photon counting error relations of Ref. 9, the error associated with laser energy measurement, and the R- and C_{F_2}-versus T curves. The Taylor series method of error propagation was used. Because Tunnel F measurements were not obtained with photon

Table 2. Tunnel C Parameters, Measured and Calculated

Data Point / DP, °F	M_1	$n_c(N_2)$, cm^{-3}	T_∞, °K	$n_m(N_2)$, cm^{-3}	T_v, °K	$S(T_v)$, percent	$u(T_v)$, percent	$S(n)$, percent	$u(n)$, percent
1 / 15	10.14	3.32×10^{17}	38	---	----	----	----	---	----
2 / 15		3.32×10^{17}	38	3.52×10^{17}	≤550	5	13	4	12
3 / 13		2.84×10^{17}	43	3.36×10^{17}					
4 / 11		2.50×10^{17}	49	2.98×10^{17}					
5 / 8		2.50×10^{17}	49	2.82×10^{17}					
6 / 10		2.50×10^{17}	49	2.74×10^{17}					
7 / 9		2.19×10^{17}	54	2.33×10^{17}					
8 / 8		2.01×10^{17}	59	2.44×10^{17}					
9 / 9				2.03×10^{17}					
10 / 8				1.86×10^{17}					
11 / -15				1.88×10^{17}	570				
12 / -21				1.84×10^{17}	650				
13 / -26				1.79×10^{17}	670				
14 / -48				2.22×10^{17}	710				
15 / -53				2.09×10^{17}	700				

Table 2. Concluded

Data Point / DP, °F	M_1	$n_c(N_2)$, cm^{-3}	T_∞, °K	$n_m(N_2)$, cm^{-3}	T_v, °K	$S(T_v)$, percent	$u(T_v)$, percent	$S(n)$, percent	$u(n)$, percent
16 / −56	10.14	2.01×10^{17}	59	2.04×10^{17}	770	5	13	4	12
17 / −58				2.19×10^{17}	790				
18 / −59				2.17×10^{17}	720				
19 / −61				2.24×10^{17}	790				
20 / −28				1.98×10^{17}	580				
21 / −55		1.83×10^{17}	56	1.72×10^{17}	760				
22 / −57		2.08×10^{17}	57	1.88×10^{17}	680				
23 / −62		2.19×10^{17}	54	2.20×10^{17}	840				
24 / −66		2.01×10^{17}	59	2.55×10^{17}	820				
25 / −66				2.45×10^{17}	800				
26 / −66				2.47×10^{17}	930				
27 / −39				2.02×10^{17}	650				
28 / −55 to −60				2.38×10^{17}	860				
29 / −61				2.17×10^{17}	820				
30 / −47				1.99×10^{17}	630				

counting instrumentation, an estimate of the photons detected was made using the known gains of the photomultipliers, the load resistances, and the peak height (volts) of the detected pulse.

Evaluation of the systematic error associated with number density measurements involves an estimate of the uncertainty associated with determination of the calibration factor C_{F_1}. It is estimated that the uncertainty of C_{F_1} is ±4 percent which will be the value assigned to the systematic error of the number density measurements.

Evaluation of the systematic error associated with the temperature measurements is rather difficult because the measurement depends on the accuracy of the theoretical calculation of intensity ratio as a function of vibrational temperature. However, the molecular constants used in the calculation are very reliable, and, as shown in Fig. 5, the

convolution calculation predicts a spectral band profile in very close agreement with the measured profile. Furthermore, the measured ratio at atmospheric calibration conditions agreed within one percent with the calculated ratio. Therefore, the systematic error of the T_v measurements is conservatively estimated at ± 3 percent.

Total uncertainty values are also listed in Tables 1 and 2 for the values measured by the laser-Raman system. Total uncertainty was calculated using the relation

$$u = \pm(B + t_{0.95} S) \tag{10}$$

The flow fields of both Tunnels F and C cannot be considered as particularly clean, because Tunnel C uses normal local air as a working gas and Tunnel F contains particulates from the arc discharge/ruptured diaphragm process. Therefore, the possible influence of laser-induced particulate incandescence (Ref. 10) on the laser-Raman results was considered. For each Tunnel C data point, the spectrometer wavelength dial was adjusted such that each detector monitored off-band radiation in the vicinity of the N_2 vibration-rotation band. Only dark count levels were detected. Because of the transient nature of the Tunnel F flow, off-band radiation measurements could not be made on the same tunnel shot for which T_v data were obtained. However, two tunnel firings were devoted to measurement of laser-induced, off-band radiation; only negligible levels were detected. Before the laser-Raman experiments in Tunnel F, Mie scattering measurements were made to determine particulate size and distribution (Ref. 11). The results of Ref. 11 indicate that copper particles of mean diameter 0.8 μm and number density of 2 x $10^4 cm^{-3}$ are present in the Tunnel F flow. Utilizing the relations developed in Ref. 10, the laser-induced incandescence photon flux was calculated and found to be negligible relative to Raman signal levels.

4.2 COMPARISON OF RESULTS WITH CALCULATIONS AND MEASURED PARAMETERS

Vibrational temperature data were obtained on three single-diaphragm runs in the Mach 8 contoured nozzle of Tunnel F. The vibrational temperature ranged from 1,650°K to 2,130°K which is nominally a factor of two higher than the bulk reservoir temperature, T_o, determined from heat probe data. From a classical point of view, if no de-excitation of the vibrational energy modes occurred in the nozzle the vibrational temperature should have been on the order of 0.6 to 0.8 times T_o. The high T_v values imply that the arc heating process leaves the gas in a nonequilibrium state which requires a long time to relax. This should not be too surprising as several investigators (Refs. 12 through 15) have discovered extreme cases of vibrational nonequilibrium in electric discharges. In Ref. 12 a flowing N_2 discharge was investigated using Raman scattering, and a vibrational temperature of

1,950°K was measured while the rotational temperature was $\cong 400°K$. In Ref. 14 Coherent Anti-Stokes Raman Spectroscopy (CARS) was used to investigate the center of a D_2 electrical discharge, and $T_v = 1,050°K$ and $T_R \cong 400°K$ were measured. In Ref. 15 CARS was used to investigate the center of an N_2 electrical discharge, and $T_v = 2,600°K$ with T_R near ambient conditions was measured. It was also found in Ref. 15 that the $v = 0,1,2$ level populations were well represented by a Boltzmann distribution, whereas the higher vibrational level populations exhibited extreme deviations from a Boltzmann distribution.

In order to provide more time for the reservoir relaxation process in Tunnel F, a run was made with the double diaphragm and the Mach 8 nozzle. A delay time, $\Delta\tau$, measured from the start of arc discharge to the rupture of the diaphragms, of 463 msec was achieved. On this run the vibrational temperature was less than 500°K, which was the limit of resolution of the laser-Raman system. This result also implies that the high vibrational temperatures seen on the single-diaphragm runs is the result of arc-induced nonequilibrium in the reservoir gas.
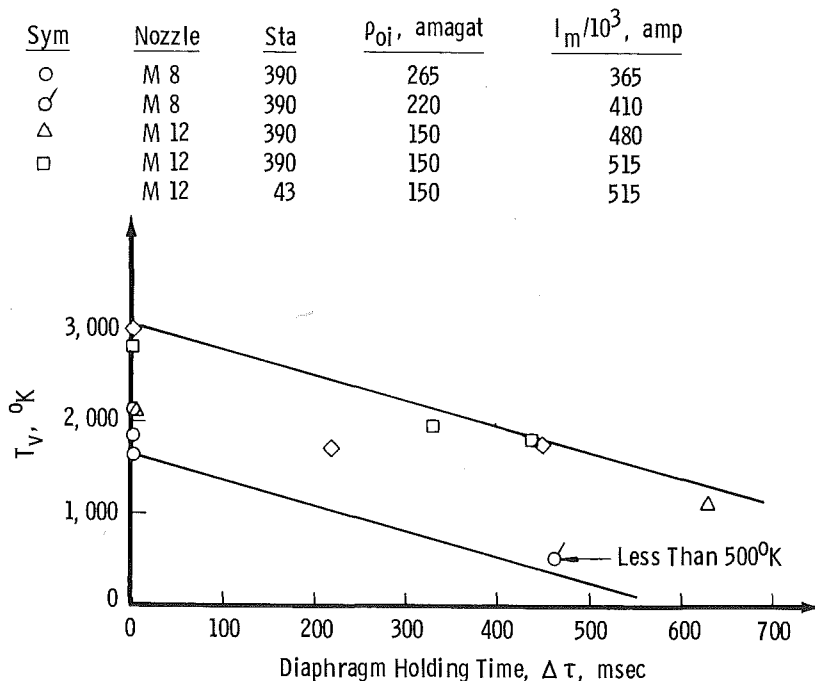
Mach numbers M_1 and M_3 are tabulated in Table 1 for the Mach 8 contoured nozzle Tunnel F runs. On the single-diaphragm runs the actual Mach number, M_3, is nominally ten percent below the pitot Mach number, M_1. On the double-diaphragm run, the actual Mach number increased to within two percent of the pitot Mach numbers measured for the other runs. Unfortunately, the added delay time resulted in overheating of the reservoir pressure transducers and the loss of the data necessary to calculate M_1 on the Mach 8 double-diaphragm run.

Vibrational temperature measurements in the Mach 12 contoured nozzle of Tunnel F also indicate T_v in the free stream to be far in excess of the bulk reservoir T_o (see Table 1). In this case, delay times up to 628 msec were not sufficient for complete relaxation of the reservoir gas; however, the 1,000°K reduction in T_v is significant. The T_v data obtained at the ablation test section shows the same behavior as the 54-in. (1.37 m)-diam test section data within experimental uncertainty.

A series of correlations of the T_v data with $\Delta\tau$, $\varrho_{oi}\Delta\tau'$ and $\varrho_{oi}\Delta\tau'/I_m$ is shown in Figs. 15a, b, and c, respectively. As observed in Fig. 15c, an excellent correlation is obtained with the product of initial arc chamber density and total delay time divided by the maximum current of the arc discharge.

Figure 16 is a plot of the ratio of measured N_2 number density to calculated N_2 number density as a function of measured vibrational temperature, where the calculated number densities are determined from M_3 measurements. The measured values show better

agreement with calculated values for the double-diaphragm runs. For the single-diaphragm runs, the ratio becomes increasingly larger than unity as T_v increases. Such results do not enhance the confidence level of free-stream property calculations based on M_3 for arc-heated flows.

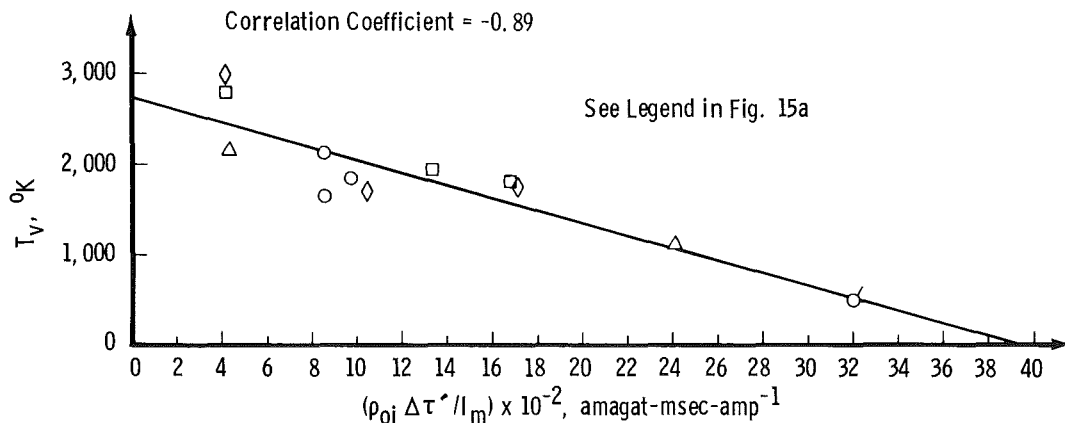| Sym	Nozzle	Sta	ρ_{oi}, amagat	$I_m/10^3$, amp
○	M 8	390	265	365
♂	M 8	390	220	410
△	M 12	390	150	480
□	M 12	390	150	515
	M 12	43	150	515

a. Effect of diaphragm holding time
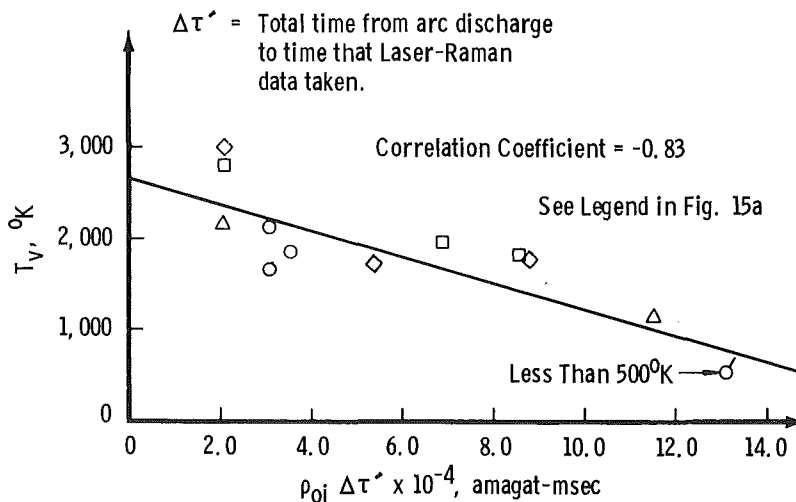
b. Correlation with time-density product

Figure 15. Effect of delay time, density, and current on
vibrational temperature, Tunnel F.

28

c. Correlation with time-density/current
Figure 15. Concluded.

Sym	Nozzle	ρ_{oi}, amagat	$I_m/10^3$, amp
○	M 8	265	365
∅	M 8	220	410
△	M 12	150	480
□	M 12	150	515

Open Sym – Single Diaphragm
Solid Sym – Double Diaphragm

$n_m(N_2)$ – Laser-Raman System
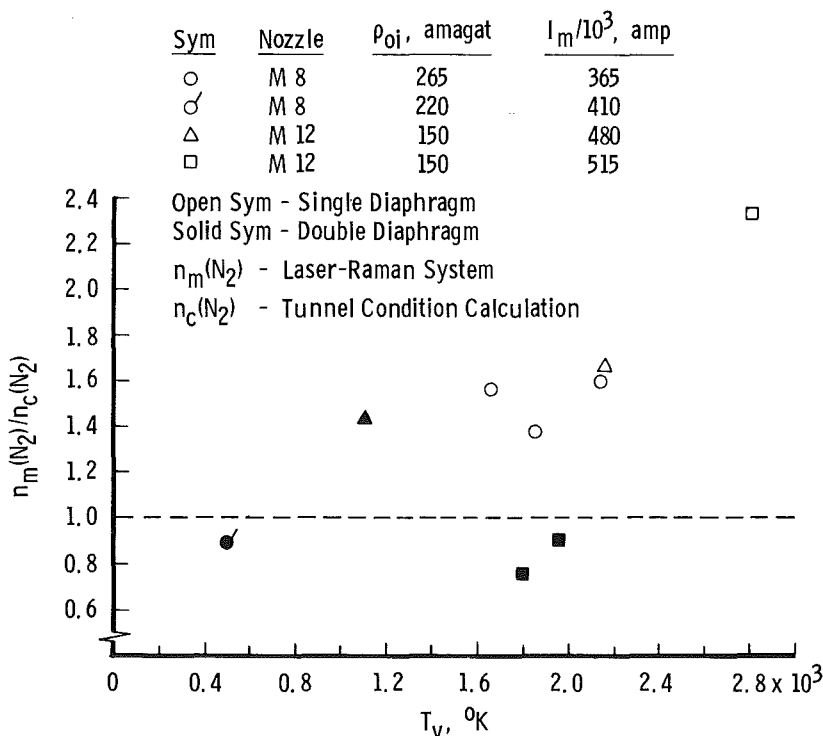$n_c(N_2)$ – Tunnel Condition Calculation

Figure 16. Free-stream N_2 number density ratio as a function of T_v, Tunnel F.

The vibrational temperatures measured in Tunnel C varied from 550°K to 930°K. A correlation of T_v and Mach number with specific humidity is shown in Figs. 17a and b. At high specific humidity, the vibrational temperature is less than 550°K which corresponds

29

roughly to the measurement threshold of the laser-Raman system. As the specific humidity decreased to a minimum of 1.4 x 10^{-5}, the vibrational temperature increased to 850°K. Simultaneously, the actual Mach Number (M_3) increased from 8.2 to 9.8; the pitot Mach number did not sense any change in flow-field conditions. The final T_v value is approximately equal to the level calculated for a nonequilibrium expansion from the reservoir conditions. The decrease in free-stream vibrational temperature with increasing humidity implies that the presence of water vapor at very low concentration results in the de-excitation of the nitrogen vibrational energy levels. Furthermore, it appears that the majority of the energy derived from the de-excitation process transfers to the translational and rotational energy modes thereby increasing static temperature and decreasing the Mach number.

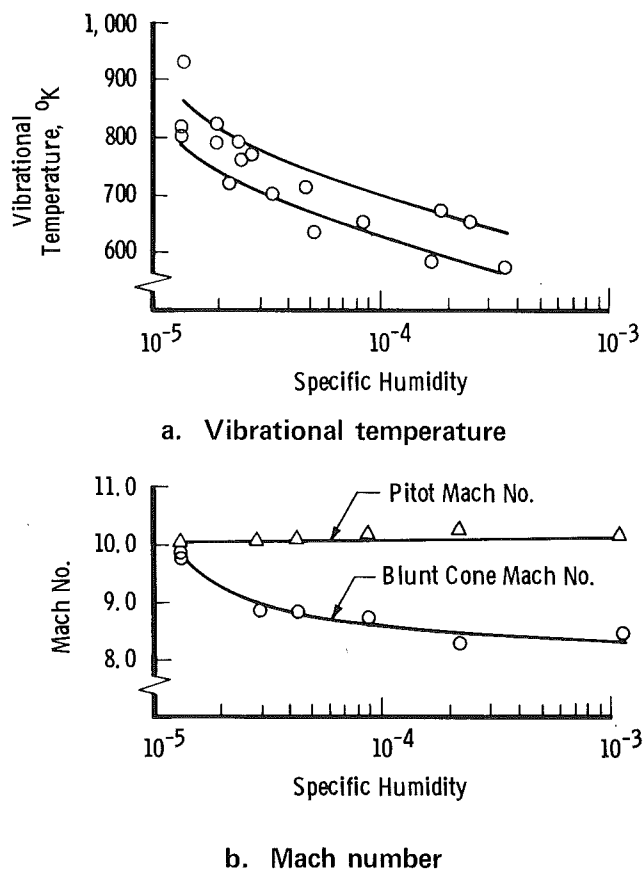a. Vibrational temperature

b. Mach number

Figure 17. Effect of water vapor on vibrational temperature and Mach number in Tunnel C.

Fig. 18 is a plot of the ratio of measured N_2 number density to calculated N_2 number density as a function of measured vibrational temperature. The calculated number densities

are based on M_1. Once again, the ratio becomes increasingly larger than unity as T_v increases.
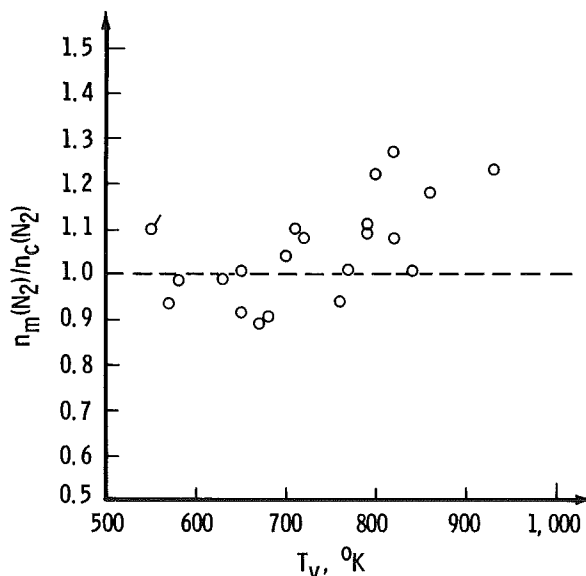

Figure 18. Free-stream N_2 number density
ratio as a function of T_v,
Tunnel C.

The experiments in Tunnel C have fostered the hypothesis that the phenomenon of decreasing free-stream Mach number with increasing specific humidity is the result of water vapor-induced de-excitation of vibrationally excited nitrogen molecules. A phenomenological diagram of the process is given in Fig. 19. The energy stored in the vibrational energy modes during the initial portion of the nozzle expansion (classical freezing process) is small compared to the overall flow energy but is large compared to the molecular translational and rotational energy in the highly expanded downstream section of the nozzle. The transfer of vibrational energy, triggered by the presence of water vapor, to the translational and rotational modes results in a significant increase in local static temperature and a corresponding reduction in Mach number. This nonisentropic process is analogous to a simple heat addition or diabatic flow process.

To assess the validity of this hypothesis, from the results in Refs. 16 and 17, it is known that the H_2O-N_2 vibrational quenching process is much more efficient than N_2-N_2 quenching. Pressure-deactivation time products ($p\tau_d$) for the H_2O-N_2 quenching process were found to be a factor of 10^{-2}-10^{-4} less than those for the N_2-N_2 quenching process and on the order of 1 to 4 μsec-atm for the 500 to 3,000°K temperature range. At 2,000°K, the quenching rate

constant for the N_2-H_2O quenching process is 1,000 times greater than the N_2-N_2 quenching process, for example. However, when the relatively small amount of H_2O in the Tunnels F and C flow fields is considered, it is obvious that H_2O-N_2 collisions could not result in the required energy transfer, and it becomes painfully obvious that the physics of the water vapor-induced de-excitation process is not understood at this time. It may be speculated that the sudden appearance of condensate clusters, generated by the homogeneous nucleation of water vapor, may play a dominant role in the de-excitation process.
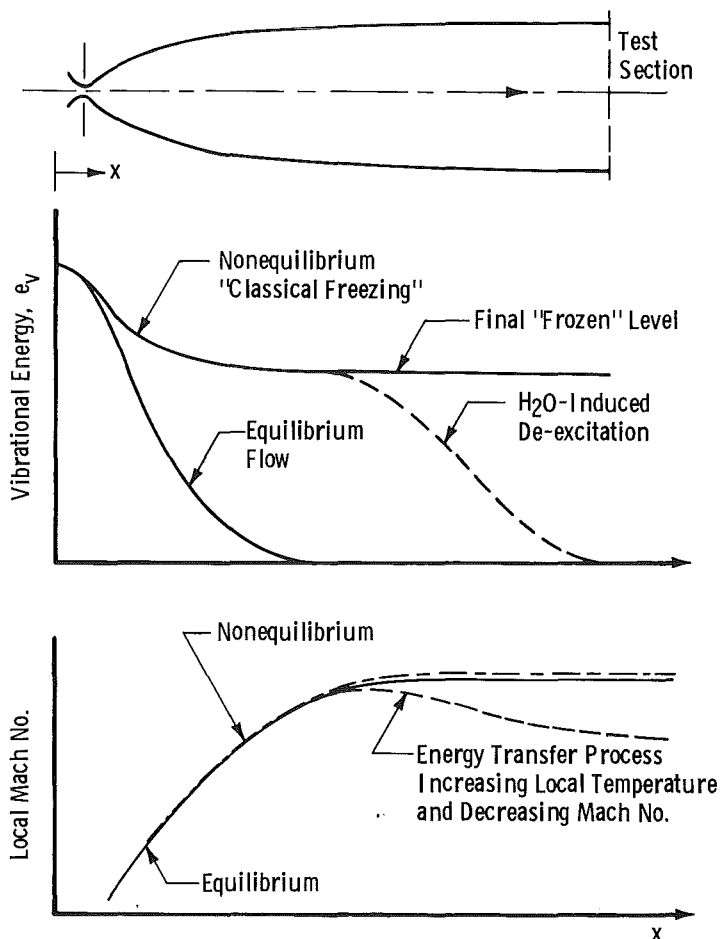

Figure 19. Effect of water vapor-induced de-excitation
of vibrational energy on Mach number.

5.0 SUMMARY OF RESULTS

An experimental investigation to determine if vibrational nonequilibrium existed in the AEDC Tunnels F and C flow fields and upon what tunnel operating parameters the degree of nonequilibrium depended has been successfully completed. The results may be summarized as follows:

1. Vibrational nonequilibrium exists in Tunnel F flow fields. For example, at the Mach 8 condition having a $T_o \approx 880°K$ and $T_\infty \approx 84°K$, vibrational temperatures of approximately 1,880°K (± 13 percent) were measured. It is speculated that a large number of low energy secondary electrons exist in the arc chamber and are the driving mechanism for the extremely high vibrational temperatures.

2. Delay of the Tunnel F nozzle expansion process with double diaphragms resulted in a significant reduction in T_v; however, complete relaxation to the equilibrium level was achieved at only one test condition in the Mach 8 contoured nozzle.

3. Measured Tunnel F T_v values plotted as a function of $\varrho_{oi} \, \Delta \tau' / I_m$ gave an excellent correlation coefficient of -0.89. This result implies that there are realizable test conditions for Tunnel F at which the Mach number problem can be minimized or eliminated.

4. Vibrational nonequilibrium exists in Tunnel C flow fields, but to a lesser extent than observed in Tunnel F. At reservoir conditions of 1,470 psia and 1,200°K, the free-stream vibrational temperature in Tunnel C was found to be approximately 900°K for low humidity ($\omega \approx 10^{-5}$) conditions. This result is consistent with classical nonequilibrium theory for expanding nozzle flow. At the standard tunnel condition ($T_o = 1,055°K$), the free-stream vibrational temperature would be less than the value observed in the present experiments.

5. The degree of vibrational nonequilibrium in Tunnel C was found to vary with the amount of water vapor in the flow field. Increasing specific humidity from $\approx 10^{-5}$ to 3.5×10^{-4} decreased the vibrational temperature from 930°K to 550°K.

6. It is speculated that condensate clusters generated by the homogeneous nucleation of water vapor play a dominant role in the de-excitation of the excited vibrational levels in Tunnel C.

7. Comparison of Mach numbers M_1 and M_3 for both tunnel flow fields reveals that M_1 results can lead to the erroneous conclusion that the flow is isentropic. When a nonisentropic process such as the water vapor-induced de-excitation of vibrationally excited molecules is present, M_3 is the more reliable Mach number because it is inferred from local measurements.

8. The increasing density ratio, $n_m(N_2)/n_c(N_2)$, with increasing T_v in both tunnel flows is troublesome, because the calculated N_2 number density value is dependent upon Mach number. This implies that static tunnel conditions calculated from the Mach number are far from accurate for certain tunnel conditions.

REFERENCES

1. Williams, W. D., Hornkohl, J. O., and Lewis, J. W. L. "Electron Beam Probe for a Low Density Hypersonic Wind Tunnel." AEDC-TR-71-61 (AD724004), July 1971.

2. Lewis, J. W. L., Williams, W. D., Price, L. L., and Powell, H. M. "Nitrogen Condensation in a Sonic Orifice Expansion Flow." AEDC-TR-74-36 (AD783254), July 1974.

3. Williams, W. D. and Lewis, J. W. L. "Rotational Temperature and Number Density Measurements of N_2, O_2, CO, and CO_2 in a Hypersonic Flow Field Using Laser-Raman Spectroscopy." AEDC-TR-75-37 (ADA012877), July 1975.

4. Lewis, J. W. L. and Williams, W. D. "Profile of an Anisentropic Nitrogen Nozzle Expansion." *The Physics of Fluids*, Vol. 19, No. 7, July 1976, pp. 951-959.

5. Placzek, G. "The Rayleigh and Raman Scattering." Translated from a Publication of the Akademische Verlagsgesellschaft G.M.B.H., Leipzig 1934, Handbuch der Radiologie, Heft 6, Teil 2, pp. 209-374.

6. Anderson, A., Ed. *The Raman Effect*, Vol. 2., Marcel Dekker, Inc., New York, 1973.

7. Powell, H. M., Williams, W. D., Jones, J. H., and McGuire, R. L. "Instrumentation for Raman/Rayleigh Light Scattering Measurements in Aerospace Test Facilities." Instrument Society of America, Transactions, Vol. 17., Number 2, 1978.

8. Klobuchar, R. L., Ahumada, J. J., Michael, J. V., and Karol, P. J. "Details of Dead Time Losses to Scaling and Multiscaling." *Rev. Sci. Instrum.*, Vol. 45, No. 9, September 1974.

9. Beers, Y. *Introduction to the Theory of Error.* Addison-Wesley Publishing Co., Inc., Reading, Massachusetts, 1953.

10. Eckbreth, A. C. "Effects of Laser-Modulated Particulate Incandescence on Raman Scattering Diagnostics." *Journal of Applied Physics*, Vol. 48, No. 11, November 1977, pp. 4473-4479.

11. Lewis, J. W. L., Curry, B. P., and Weaver, D. P. "Determination of the Size Distribution Function for Particles in a Hypersonic Flow Field." AEDC-TR-77-101 (ADA056923), July 1978.

12. Nelson, L. Y., Saunders, A. W., Jr., and Harvey, A. B. "Detection of Vibrationally Excited Homonuclear Diatomic Molecules by Raman Spectroscopy." *Journal of Chemical Physics*, Vol. 55, No. 10, November 1971, pp. 5127-5128.

13. Nibler, J. W., McDonald, J. R., and Harvey, A. B. "Coherent Anti-Stokes Raman Spectroscopy of Gases." *Optics Communications* Vol. 18, No. 1, July 1976, p. 134.

14. Nibler, J. W., McDonald, J. R., and Harvey, A. B. "CARS Measurement of Vibrational Temperatures in Electric Discharges." *Optics Communications*, Vol. 18, No. 3, August 1976, pp. 371-373.

15. Shaub, W. M., Nibler, J. W., and Harvey, A. B. "Direct Determination of Non-Boltzmann Vibrational Level Populations in Electric Discharges by CARS." *Journal of Chemical Physics*, Vol. 67, No. 5, September 1977, pp. 1883-1886.

16. Whitson, M. E., Jr. and McNeal, R. J. "Temperature Dependence of the Quenching of Vibrationally Excited N_2 by NO and H_2O." *Journal of Chemical Physics*, Vol. 66, No. 6, March 1977, pp. 2696-2700.

17. Center, R. E. and Newton, J. F. "Vibrational Relaxation of N_2 by H_2O." *Journal of Chemical Physics*, Vol. 68, No. 8, April 1978, pp. 3327-3333.

NOMENCLATURE

B	Systematic error, percent
C	Constant defined by Eq. (8)
C_{F_1}	Calibration constant for measurement of $n(N_2)$ as defined by Eq. (3)
C_{F_2}	Calculated temperature-dependent factor used for measurement of $n(N_2)$
DP	Dewpoint, °F
E_{vac}, E	Transmitted laser energy at vacuum conditions, and transmitted laser energy at other than vacuum conditions, respectively
e_v	Vibrational energy
$I(v = 0)$, $I(v = 1)$	Raman scattered intensity of the $v = 0$ and $v = 1$ vibrational levels, respectively
I_m	Initial arc current, amps
M	Mach number
M_1, M_3	Pitot Mach number and actual Mach number, respectively
$n(N_2)$	Nitrogen number density, cm^{-3}
p_c	Cone surface pressure
p_n	Nozzle wall static pressure
p_o	Reservoir pressure
p_o'	Pitot pressure
p_∞	Free-stream pressure

R	Raman scattered intensity ratio, $I(v = 1)/I(v = 0)$
R_R	Relative sensitivity of two detector channels
S	Random error, percent
T_F	Laser beam transmission factor defined by Eq. (4)
T_o	Reservoir temperature, °K
T_R	Rotational temperature, °K
T_v	Vibrational temperature, °K
T_∞	Free-stream static temperature, °K
t	Time
$t_{0.95}$	Student's 95-percent confidence limit
u	Total uncertainty, percent
v	Vibrational level quantum number
$\Delta\tau$	Diaphragm holding time measured from the start of arc discharge to diaphragm rupture, sec
$\Delta\tau'$	Delay time measured from the start of arc discharge to time of T_v data acquisition, sec
λ	Wavelength, Å
ϱ_{oi}	Initial Tunnel F reservoir density, amagats
τ_D	Photon counting dead time, sec
τ_g	Photon counting data acquisition duration, sec
ω	Specific humidity

SUBSCRIPTS

c   Indicates a calculated value

m   Indicates a measured value

SUPERSCRIPTS

$^\circ$ Indicates calibration conditions in effect

t   Indicates test conditions in effect